Discovery, design, and synthesis of anti-metastatic lead phenylmethylene hydantoins inspired by marine natural products

Mudit, M.; Khanfar, M.; Muralidharan, A.; Thomas, S.; Shah, G.V.; van Soest, R.W.M.; El Sayed, K.A.

DOI
10.1016/j.bmc.2008.12.053

Publication date
2009

Published in
Bioorganic & Medicinal Chemistry

Bioorganic & Medicinal Chemistry 17 (2009) 1731–1738

Contents lists available at ScienceDirect

Bioorganic & Medicinal Chemistry

journal homepage: www.elsevier.com/locate/bmc

Discovery, design, and synthesis of anti-metastatic lead phenylmethylene hydantoins inspired by marine natural products

Mudit Mudit [a], Mohammad Khanfar [a], Anbalagan Muralidharan [a], Shibu Thomas [a], Girish V. Shah [a], Rob W. M. van Soest [b], Khalid A. El Sayed [a,*]

[a] Department of Basic Pharmaceutical Sciences, College of Pharmacy, University of Louisiana at Monroe, 1800 Bienville Drive, Monroe, LA 71201, USA
[b] Zoological Museum, University of Amsterdam, PO Box 94766, 1090 GT Amsterdam, The Netherlands

ARTICLE INFO

Article history:
Received 25 October 2008
Revised 12 December 2008
Accepted 14 December 2008
Available online 29 December 2008

Keywords:
Red Sea sponge *Hemimycale arabica*
Phenylmethylene hydantoins
Prostate cancer
Anti-metastatic
Spheroid disaggregation
Comparative molecular field analysis
3D QSAR

ABSTRACT

The Red Sea sponge *Hemimycale arabica* afforded the known (*Z*)-5-(4-hydroxybenzylidene)-hydantoin (**1**), (*R*)-5-(4-hydroxybenzyl)hydantoin (**2**), and (*Z*)-5-((6-bromo-1*H*-indol-3-yl)methylene)-hydantoin (**3**). The natural phenylmethylene hydantoin (PMH) **1** and the synthetic (*Z*)-5-(4-(ethylthio)benzylidene)-hydantoin (**4**) showed potent in vitro anti-growth and anti-invasive properties against PC-3M prostate cancer cells in MTT and spheroid disaggregation assays. PMHs **1** and **4** also showed significant anti-invasive activities in orthotopic xenograft and transgenic mice models. To study the effect of electronic and lipophilic parameters on the activity, a wide array of several substituted aldehydes possessing electron-withdrawing (+σ), lipophilic (+π), electron-donating (−σ), and less lipophilic substituents (−π) were used to synthesize several PMHs. Few *des*-phenylmethylenehydantoins and 2-thiohydanoins were also synthesized and the anti-invasive activities of all compounds were evaluated. Comparative molecular field analysis (CoMFA) was then used to study the 3D QSAR. Predictive 3D QSAR model with conventional r^2 and cross validated coefficient (q^2) values up to 0.910 and 0.651 were established. In conclusion, PMH is a novel antimetastatic lead class with potential to control metastatic prostate cancer.

1. Introduction

Prostrate cancer is the most prevalent cancer form in men and constitutes the second leading cause of cancer deaths in men in United States.[1] Later stages of prostate cancer progress to life-threatening, androgen-independent and fatal metastatic forms.[2] Patient progression at metastatic stage of disease is very poor, and currently few options are available for the treatment at this stage.[1,2] Therefore, morbidity and mortality can be remarkably reduced by attenuation of metastasis.

The sponge genus *Hemimycale* (family Mycalidae) is well known for its bioactive secondary metabolites especially biogenetically complex guanidine alkaloids.[3,4] Ptilomycalin A_1 has a unique polycyclic guanidine skeleton with a spermidine group linked to a 16-hydroxyhexadecanoic acid moiety.[3–5] This novel guanidine alkaloid possesses remarkable antifungal, antiviral, and antitumor activities.[3–5]

Ethanolic extract of abundant shallow water Red Sea sponge *H. arabica* was targeted because it inhibited the proliferation and invasion of the highly metastatic human prostate cancer PC-3M cell line. Interestingly, the chemistry of this particular *Hemimycale* species was never investigated. Liquid chromatography of this extract afforded the known (*Z*)-5-(4-hydroxybenzylidene)-hydantoin (**1**),[6] (*R*)-5-(4-hydroxybenzyl)hydantoin (**2**),[7] and (*Z*)-5-((6-bromo-1*H*-indol-3-yl)methylene)-hydantoin (**3**).[8] PMH **1** was reported as a natural product from the Red Sea sponge *Laxosubrites* sp. without any biological activity.[9]

The natural PMH **1** and the synthetic **4** showed potent in vitro anti-growth and anti-invasive properties against PC-3M prostate cancer cells in MTT and spheroid disaggregation assays.[10] PMH **1** and **4** also showed anti-invasive activity in orthotopic xenograft of PC-3M cells in nude mice model.[10] They decreased orthotopic tumor growth and inhibited the formation of tumor micrometastases in distant organs without apparent cytotoxic effects at the test doses.[10] PMH **4** also showed potent activity in LPB-Tag mice transgenic model.[10] Prostate tumors of LPB-Tag mice display significant similarities with human tumors including tumor heterogeneity, neuroendocrine features and relatively slower tumor growth.[10] PMH **4** remarkably reduced growth of primary tumors and their metastasis in reproductive organs, decreased morbidity and increased survival of the LPB-Tag mice. Therefore, PMH **1** and **4** were suggested as potent attenuators of the disassembly of junctional complexes which are key events in the progression of a localized prostate tumor to its metastatic form.[10] PMH **1** and **4** are novel leads appropriate for future development as treatment for

* Corresponding author. Tel.: +1 318 342 1725; fax: +1 318 342 1737.
E-mail address: elsayed@ulm.edu (K.A.El. Sayed).

0968-0896/$ - see front matter © 2008 Elsevier Ltd. All rights reserved.
doi:10.1016/j.bmc.2008.12.053

metastatic prostate cancer and a chemopreventive agent.[10] This study represents the first structure–activity relationship study of phenylmethylene hydantoins as a novel anti-metastatic class.

The cyclic imide hydantoins are well investigated for their anticonvulsant activity.[11,12] Various pharmacological activities were reported for hydantoins including fungicidal, herbicidal, anti-inflammatory, anti-HIV, analgesic, cannabinoid receptor-1 (CB-1), 5HT, purine P-2X receptor antagonism, platelet aggregation inhibition, anti-arrhythmic and antihypertensive, anti-diabetic, neuroprotective, HDL/cholesterol modulating, antiviral, and growth hormone secretagogue.[12] Phenytoin and PMHs were previously reported to possess anticonvulsant properties.[11,12] It was also established that for the anticonvulsant activity hydantoin nucleus and phenyl ring in PMH served the basic structural requirement.[12] Several PMHs were synthesized earlier for investigating the influence of various substitutions in the phenyl ring of PMH. Maximal electroshock seizure (MES) assay was used for the evaluation of anticonvulsant activity for these compounds, and response score of 2.5 was considered equivalent to its effective dose.[11]

Occasionally, hydantoin analogs were reported to show antitumor activities. Hydantoins were shown to modulate Pg–P and inhibit MMPs.[12] Substituted diisopropylbenzylidene hydantoins and 2-thiohydantoins were patented in 1987 for their tyrosine kinase inhibitory and antiallergic activities.[13] These compounds were potent at 100 μM dose in guinea pigs.[13] 2-[4-[(5-Oxo-2-thioxo-4-imidazolidinylidene)-methyl]phenoxy] propionic acid and related analogs were patented for their ability to inhibit substrate binding by extracellular signal-regulated kinases by binding docking domains.[14] This compound blocked the interaction of extracellular signal-regulated kinases (ERK kinases) with substrate proteins, and hence considered as a possible treatment for neoplasms associated with abnormal ERK kinase activity.[14] 2-[4-[(5-Oxo-2-thioxo-4-imidazolidinylidene)-methyl]phenoxy] propionic acid and its analogs bind with the ERK1 or ERK2 kinase, inhibit phosphorylation, and suppresses cell proliferation in vitro.[14] Peptide hydantoin analogs were patented for their ability to inhibit thrombocyte aggregation, metastasis, and osteoclast binding to bone surfaces.[15] Though not typically hydantoin, but structurally related to **1**, the imidazol-2-amine, 5-chloro-*N*-(4-methylphenyl)-4-(phenylmethylene) was patented for its in vitro anti-melanoma activity.[15] Some 1-phenethyl and 5-(*E*)-benzylidene hydantoins inhibited EGFR autophosphorylation and polyGAT phosphorylation and were found to inhibit the growth and proliferation of human A-431 cells.[16] Therefore, these hydantoins were considered good scaffolds for future design of tyrosine kinase inhibitors.[16]

Limited sustainable supply of most bioactive natural products is the main obstacle that may hinder further development as drug leads.[17–19] Feasible regioselective and cost effective synthesis of the pharmacologically active marine natural product **1** not only secured adequate supply for in vitro and animal studies but it also allowed the synthesis of several related analogs for the structure-activity relationship study.[11] Several PMHs were previously synthesized to establish the anticonvulsant structure-activity relationship of this class.[11,12,20–22] This study reports the synthesis of forty PMHs and the novel report of their anti-invasive and junctional complexes stabilization activities. Only PMHs with $ED_{MES(2.5)} > 200$ mg/kg in MES assay were selected to avoid the possibility of potential central nervous system effects.[11] 3D-QSAR Model was established and validated.

2. Results and discussion

Three known hydantoins (**1–3**) were isolated from the Red Sea sponge *H. arabica*. Among these, (*Z*)-5-(4-hydroxybenzylidene)hydantoin (**1**) was found to be the most active one against proliferation, invasion, and junctional complexes destabilization of PC-3M cells.[10–12]

Eight new compounds (**4**-**11**) were synthesized along with thirty-one other known PMHs (**12**-**42**) using the base-catalyzed condensation reaction of hydantoin with different substituted benzaldehydes in the presence of ethanolamine (Scheme 1).[11,12]

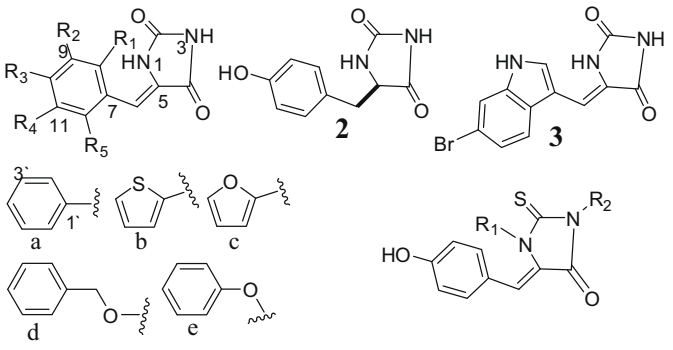

The HREIMS data of **4** showed a molecular ion peak at *m/z* 248.0622, suggesting the molecular formula $C_{12}H_{12}N_2O_2S$. ^1H and ^{13}C NMR data (Tables 1 and 2) analysis indicated that **4** is (*Z*)-5-(4-(ethylthio)benzylidene)imidazolidine-2,4-dione. The olefinic proton singlet at δ 6.36 which correlated with the methine carbon at δ 108.2 was assigned H-6. Proton H-6 showed ^3J-HMBC correlations with the amide carbonyl C-4 (δ 166.5) and the aromatic methine carbons C-8 and C-12 (δ 130.4), confirming the phenylmethylene hydantoin entity of **4**. H-6 also showed ^2J-HMBC correlations with the quaternary carbons C-5 and C-7 (δ 137.8 and 128.3, respectively). Protons H-8 and H-12 showed COSY correlations with protons H-9 and H-11, respectively (Table 1). Protons H-8 and H-12 also showed ^3J-HMBC correlations with the quaternary carbon C-10 (δ 130.5). The methyl triplet H_3-2′ (δ 1.23) showed COSY coupling with the methylene quartet H_2-1′ (δ 3.02). H_2-1′ also showed ^3J-HMBC correlation with the quaternary aromatic carbon C-10 (δ 130.5). The later carbon was assigned based on its ^3J-HMBC correlation with protons H-8 and H-12.

The HREIMS data of **5** showed a molecular ion peak at *m/z* 238.0559 and suggested a molecular formula of $C_{11}H_8F_2N_2O_2$. ^1H and ^{13}C NMR data of **5** (Tables 1 and 2) confirmed the identity of 2,3-difluoro-4-methylbenzylidene moiety. The olefinic proton singlet H-6 showed ^3J-HMBC correlations with the quaternary aromatic C-8 (δ 148.1) and the methine aromatic C-12 (δ 124.4). Proton H-12 showed ^3J-HMBC correlations with the quaternary aromatic carbons C-8 and C-10 (δ 127.3). The methyl singlet H_3-1′ (δ 2.29) showed a ^2J-HMBC correlation with the quaternary aromatic C-10 (δ 127.3) and ^3J-HMBC correlations with the quaternary aromatic carbon C-9 (δ 149.0) and the methine aromatic carbon C-11 (δ 126.7). It is worth noting that the 8,9-difluoro substitution remarkably affected the splitting of aromatic protons and carbons. In addition to expected *o*-coupling (J = 7.6 Hz), each of H-11 and H-12 also showed ^4J-coupling (J = 4.4 Hz) with C-9 and C-8 fluoro moieties, respectively. Each of carbons C-7 and C-10 splitted as doublet (J = 9.9 and 13.8 Hz, respectively) due to ^2J-coupling with C-8 and C-9 fluoro groups, respectively. Similarly, each of carbons

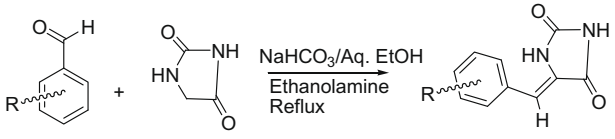

Scheme 1. General synthetic scheme of phenylmethylene hydantoins.[11]

Table 1
^{1}H NMR data of compounds **4**–**7**[a]

Position	δ_H			
	4	**5**	**6**	**7**
6	6.36, s	6.31, s	6.19, s	6.50, s
7	—	—	—	—
8	7.56, d (8.4)	—	—	7.83, br s
9	7.28, d (8.4)	—	7.72, m	—
10	—	—	7.43, m	7.60, d (7.7)
11	7.28, d (8.4)	7.12, dd (7.6, 4.4)	7.41, m	7.41, m
12	7.56, d (8.4)	7.45, dd (7.6, 4.4)	7.34, m	7.60, d (7.7)
1′	3.02, q (7.4)	2.29, 3H, s	—	—
2′	1.23, t (7.4)	—	7.42, 2H, d (8.8)	7.74, 2H, d (7.4)
3′	—	—	7.33, 2H, dd (8.8, 8.0)	7.51, m
4′	—	—	7.48, m	7.41, m
5′	—	—	7.33, 2H, dd (8.8, 8.0)	7.51, m
6′	—	—	7.42, 2H, d (8.8)	7.74, 2H, d (7.4)

[a] In DMSO, 400 MHz. Coupling constants (*J*) are in Hertz.

Table 2
^{13}C NMR data of compounds **4**–**7**[a]

Position	δ_C			
	4	**5**	**6**	**7**
2	156.6, qC	156.8, qC	156.2, qC	156.4, qC
4	166.5, qC	166.3, qC	165.9, qC	166.2, qC
5	137.8, qC	131.4, qC	129.3, qC	128.8, qC
6	108.2, CH	97.9, CH	107.4, CH	108.8, CH
7	128.3, qC	121.3, qC	140.5, qC	140.3, qC
8	130.4, CH	148.1, qC	142.5, qC	128.0, CH
9	127.8, CH	149.0, qC	129.5, CH	141.4, qC
10	130.5, qC	127.3, qC	128.3, CH	129.0, CH
11	127.8, CH	126.7, CH	128.1, CH	128.2, CH
12	130.4, CH	124.4, CH	130.6, CH	129.0, CH
1′	26.0, CH_2	14.6, CH_3	131.1, qC	134.2, qC
2′	14.6, CH_3	—	129.0, CH	127.6, CH
3′	—	—	130.1, CH	129.4, CH
4′	—	—	129.1, CH	128.2, CH
5′	—	—	130.1, CH	129.4, CH
6′	—	—	129.0, CH	127.6, CH

[a] In DMSO, 100 MHz. Carbon multiplicities were determined by APT experiments. qC = quaternary, CH = methine, CH_2 = methylene, CH_3 = methyl carbons.

C-8 and C-9 splitted as doublet of doublets (*J* = 247.0, 13.0 and 242.0, 11.9 Hz, respectively) due to ^{1}J and ^{2}J coupling with C-8 and C-9 fluoro groups.[23,24]

The ^{1}H and ^{13}C NMR data of **6** and **7** (Tables 1 and 2) as well as their HREIMS suggested close similarity to **1** with an additional phenyl moiety. The location of this phenyl group whether at C-8 in **6** or at C-9 in **7** was based on HMBC and COSY data.

The ^{1}H and ^{13}C NMR data of **8** and **9** (Tables 3 and 4) as well as their HREIMS suggested close similarity to **1** with an additional 2-thienyl moiety. The location of this new thienyl group whether at C-8 in **8** or at C-10 in **9** was based on HMBC data. The quaternary carbon C-2′ (δ 141.5) of the thiophene ring in **8** was assigned based on its ^{3}*J*-HMBC correlation with the aromatic proton H-9. Proton H-5' (δ 7.62) showed ^{3}*J*-HMBC correlations with C-2′ and C-3′, in addition to a ^{2}*J* HMBC correlation with C-4'. Proton H-3′ (δ 7.51) showed a ^{3}*J*-HMBC correlation with C-8 (δ 134.5) which confirmed the position of thiophene ring.

The ^{1}H and ^{13}C NMR data of **10** (Tables 3 and 4) along with its HREIMS suggested similarity to **1** with an additional 2-(furan-2-yl) functionality. The carbon C-2′ of furan ring showed ^{3}*J*-HMBC correlations with Proton H-9 of benzene ring, and also with protons H-4′ and H-5′. Connection of the furan ring to the benzene ring was also confirmed by the ^{3}*J*-HMBC correlation of H-3′ with the quaternary aromatic C-8 (δ 130.0).

The IR spectrum of **11** showed a ν_{max} band at 2235 cm^{-1}, suggesting the presence of cyano functionality.[25] The ^{1}H and ^{13}C NMR data of **11** (Tables 3 and 4) along with its HREIMS suggested similarity to **1** with an additional 9-cyano functionality. The quaternary carbon at δ 119.1 was assigned as the cyano carbon C-1′ based on its ^{3}*J*-HMBC correlation with proton H-10 (δ 7.74).

The loss of cell–cell adhesion is associated with tumor metastasis in several epithelial cancers including prostate, breast and renal carcinomas.[26,27] Thus compounds which strengthen cell–cell adhesion can potentially serve as possible therapies for advanced prostate cancer.[28] PC-3M prostrate cancer cells used in this study were

Table 3
^{1}H NMR data of compounds **8**–**11**[a]

Position	δ_H			
	8	**9**	**10**	**11**
6	6.45, s	6.43, s	6.55, s	6.39, s
7	—	—	—	—
8	—	7.68, 2H, m	—	8.12, s
9	7.68, m	7.66, 2H, m	7.69, dd (1.8, 7.5)	—
10	7.40, m	—	7.43, ddd (7.7, 7.6, 1.5)	7.74, br d (8.0)
11	7.18, m	7.66, 2H, m	7.39, ddd (7.7, 7.6, 1.5)	7.58, dd (7.7, 7.7)
12	7.42, m	7.68, 2H, m	7.62, dd (7.5, 1.8)	7.89, br d (8.0)
1′	—	—	—	—
2′	—	—	—	—
3′	7.51, m	7.59, dd (5.1, 1.1)	6.67, dd (3.3, 0.8)	—
4′	7.17, m	7.16, dd (5.1, 3.7)	6.65, dd (3.3, 1.8)	—
5′	7.67, m	7.62, dd (3.7, 1.1)	7.85, dd (1.8, 0.8)	—
6′	—	—	—	—

[a] In DMSO, 400 MHz. Coupling constants (*J*) are in Hertz.

Table 4
^{13}C NMR data of compounds **8**–**11**[a]

Position	δ_C			
	8	**9**	**10**	**11**
2	156.2, qC	156.3, qC	156.1, qC	159.2, qC
4	165.9, qC	166.1, qC	165.9, qC	170.6, qC
5	130.0, qC	128.4, qC	79.7, qC	130.6, qC
6	107.1, CH	108.2, CH	107.2, CH	105.8, CH
7	131.4, qC	132.6, qC	130.4, qC	134.9, qC
8	134.5, qC	130.7, CH	130.0, qC	132.5, CH
9	128.0, CH	126.0, CH	127.7, CH	112.5, qC
10	129.2, CH	134.0, qC	128.5, CH	131.9, CH
11	128.5, CH[b]	126.0, CH	129.1, CH	130.4, CH
12	128.7, CH	130.7, CH	130.1, CH	134.6, CH
1′	—	—	—	119.1, qC
2′	141.5, qC	143.2, qC	152.0, qC	—
3′	130.7, CH	126.8, CH	112.6, CH	—
4′	128.6, CH[b]	129.2, CH	111.2, CH	—
5′	130.0, CH	124.9, CH	130.1, CH	—

[a] In DMSO, 100 MHz. Carbon multiplicities were determined by APT experiments. qC = quaternary, CH = methine carbons.
[b] Interchangeable.

derived from liver metastasis of PC-3 xenografts.[29,30] Studies have shown that calcitonin (CT) significantly increases tumor growth and metastasis of PC cell lines.[29,30] These effects may be mediated by the disruption of cell-cell adhesion.[29,30] A dose of 50 nM CT was optimal for stimulation of PC-3M cell proliferation and invasion.[10] A 50 μM dose of PMH **1** remarkably reduced CT-stimulated proliferation increase and displayed minimal cytotoxic effect on PC-3M cells as suggested by no decrease in cell viability in MTT assay.[10] The same dose of PMH **1** significantly increased transepithelial resistance of (TER) diluent and CT-treated PC-3M cultures, suggesting that **1** promotes tight junctions (TJs) formation and completely reverses the actions of CT on TER.[10] PMH **1** also decreased baseline and abolished CT-induced increase in paracellular permeability of polarized PC-3M cell layers.[10] This effect further supported the fact that **1** promotes TJs formation.[10]

Intraperitoneally-administered to orthotopic PC-3M-CT+ xenografts in nu/nu nude mice, PMHs **1** and **4** significantly reduced and localized the tumor mass in the abdominal cavity and prevented the formation of distant metastases at a dose of 5 or 1 μg/g body weight/day, respectively, compared to diluent-treated mice in a 60-days in vivo study.[10,31,32] Both **1** and **4** remarkably decreased the metastasis of PC-3M-CT+ cells in most organs, and reduced size of tumor cell colonies in organs where metastases were present.[10,31,32] Three equally divided intraperitoneal doses of 2 μg of **4**/g body weight/week remarkably reduced growth of primary tumors and their metastasis in reproductive organs, decreased morbidity and increased survival of LPB-Tag transgenic mice.[10]

2.1. Molecular modeling and CoMFA analysis

Based on the aforementioned results, PMHs are considered potential leads for the control and prevention of metastatic prostate cancer. To establish the structure–activity relationship of this class, a wide array of several substituted aldehydes possessing electron-withdrawing (+σ), lipophilic (+π), electron-donating (−σ), and less lipophilic substituents (−π) were used to synthesize diverse PMHs **4**-**42**, which were then tested for their anti-metastatic activity. Spheroid disaggregation assay was selected to asses this activity.[29,32–34] Since tumor cells are generally released in clumps, attach to the preferred extracellular matrix (ECM), and then radially migrate in all directions, spheroid disaggregation assay was considered a better in vitro model of tumor metastasis compared to the linear invasion assays.[29,32–34] To avoid repeated addition of exogenous CT during long incubation period of 48 h, PC-3M-CT+ cells were used because they secrete large amounts of CT and have CTR.[29] Most known PMHs including **1** and **12**-**42** showed no significant cytotoxic effects in the CNS or other organs when tested in animals at doses >100 μM.[11] Moreover, PMH **1** did not display observable toxic effects on prostate cancer cells at doses up to 200 μM in spheroid disaggregation assays (no observed dead cells) or up to 50 μM in MTT assays. We tested the anti-invasive effects of PMHs at 200 μM in spheroid disaggregation assays to observe (1) anti-invasive effects of these compounds at that dose relative to the PMH **1**; and (2) to ensure that the compound does not have significantly greater cytotoxic effects. If a PMH was not active at this particular dose it was deemed inactive. Both **1** and **4** inhibited PC-3M-CT+ spheroid disaggregation and cell migration in a dose-dependent manner with EC_{50} of 150 and 30 μM, respectively (Fig. 1). As depicted in Figure 1, the spheroid is represented by a core sphere, from which the cells migrate radially to expand the area occupied by cells (as depicted by arrow). Addition of PMH **1** or related PMHs does not affect the core spheroid, but remarkably reduce the surface area increase caused by spheroid disaggregation with time, and migration of cells in all directions (represented by arrows). The results showed that spheroid disaggregation as well as migration of cells declined in the presence of PMH derivatives in a dose-dependent manner, and the core spheroid was unchanged even after 48 h when incubated with 100 μM PMH or greater. This was not associated with cytotoxicity since PMH **1** did not affect cell viability in MTT assay. The anti-metastatic activities of synthetic PMHs **4**-**42** using spheroid disaggregation assay are shown in Tables 5 and 6. Comparative molecular field analysis (CoMFA) was used to study the 3D QSAR.[35,36] Predictive 3D QSAR model with conventional r^2 and cross validated coefficient (q^2) values up to 0.910 and 0.651, respectively, were established. The results of the CoMFA studies are summarized in Table 7. CoMFA-derived QSAR shows a good q^2 and therefore indicates a considerable predictive and correlative capacity of the model. Analysis yielded q^2 of 0.651 (3 pc) and a conventional r^2 of 0.91. A high bootstrapped (100 runs) r^2 of 0.933 (0.036) adds a high confidence limit to this analysis.

Figure 2 displays a plot of predicted versus actual activities of PMHs training set used in building a QSAR model, and the error bars depict the standard error. In this analysis both steric and electrostatic fields contribute to the QSAR equation by 70.6% and 29.4%, respectively. This suggested that variation in biological

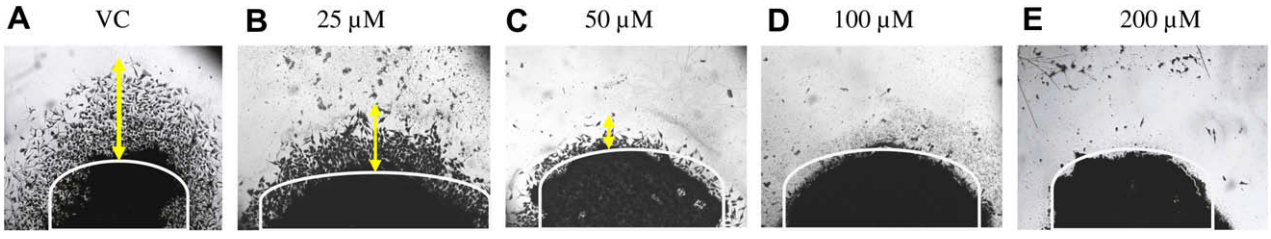

Figure 1. Spheroid disaggregation of PC-3M-CT+ prostate cells after 24 h of incubation with different doses of **4**. VC = Vehicle control. Magnification = 100x.

Table 5
Actual (200 μM dose) and predicted activity of training set[a]

Tested compound	Actual activity[b] (μm)	Predicted activity[c] (μm)
1	79	42
4	15.5	18
5	175	167
7	76	70
8	50	67
9	39	38
11	195	185
12	58	62
13	125	106
14	90	96
15	89	68
17	130	112
18	91	96
20	117	115
22	29	27
23	94	114
24	112	109
26	115	109
31	89	94
32	87	70
33	65	81
34	145	124
35	106	122
36	90	74
37	91	92
38	82	69
39	86	92
41	135	161
42	138	134

[a] Migration value for control group 180 μm.
[b] Measured from spheroid disaggregation assay.
[c] Calculated using the PLS equation of CoMFA.

Table 6
Actual (200 μM dose) and predicted activity of test set[a]

Tested compound	Actual activity[b] (μm)	Predicted activity[c] (μm)
6	56	62
10	186	160
28	116	122
29	26	43
30	87	99
40	55	79

[a] Migration value for control group 185 μm.
[b] Measured from spheroid disaggregation assay.
[c] Calculated from the PLS equation of CoMFA.

Table 7
Summary of CoMFA results

Statistical parameter	Value
q^2	0.651
r^2 Conventional	0.910
Std. error	0.115
No. of comp.	3
F value	84.092
P value	0.000
Steric contrib.	0.706
Electrostatic contrib.	0.294
r^2_{pred}	0.686
r^2_{bs} (SD)	0.933 (0.036)

activity of inhibitors is dominated by differences in steric (van der Waals) interactions with the hydantoins active site. This analysis predicted the activities of the molecules of test set with r^2_{Pred} of 0.686. Figure 3 shows the plot of predicted versus observed activities of the test set.[35,36]

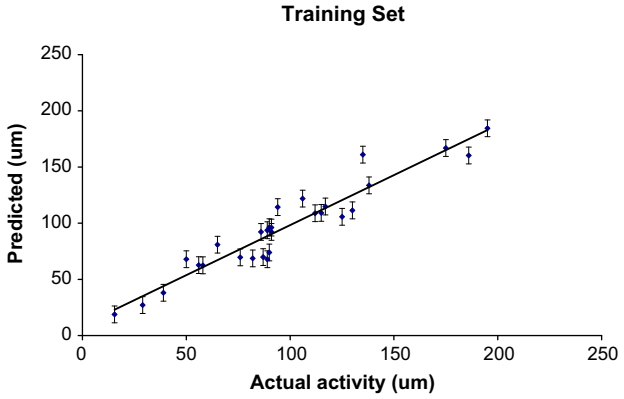

Figure 2. Predicted versus actual activity of selected PMHs training set; standard errors are shown as error bars.

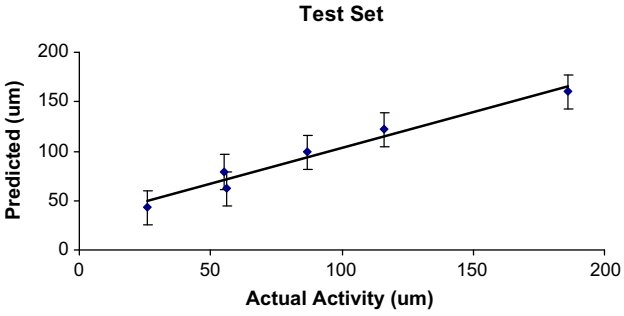

Figure 3. Predicted versus actual activity of selected PMHs test set; standard errors are shown.

The leave-one-out cross-validation method might lead to high q^2 values which do not necessarily reflect a general predictability of the models. Therefore, cross-validation was performed using two groups (leave-half-out). In this method, 50% of the PMHs were randomly selected and a model was generated, which was then used to predict the activity of the remaining 50% of compounds. The random formation of the cross-validation groups may have an effect on the results and therefore cross-validation was performed 100 times for all the analyses. The mean q^2 value was 0.613 which is slightly lower compared to the values obtained with the leave-one-out method. In no case were q^2 values negative. The obtained results suggest that there is a good internal consistency in the underlying data set. Figure 4 shows the superposition of the PMHs training and test sets.

To visualize the CoMFA steric and electrostatic fields from PLS analysis, contour maps of the product of the standard deviation associated with the CoMFA column and coefficient (SD × coeff) at each lattice point were generated (Fig. 5). The contour maps are plotted as percentage contribution to the QSAR equation and are associated with the differences in biological activity. The most active PMH **4** is displayed in the contour maps of QSAR model (Fig. 5). The regions of high and low steric tolerance are shown in green and yellow polyhedra, respectively (Fig. 5A). Areas of high steric bulk tolerance (80% contribution) were observed near the *p*-position of the benzylidene group in **4**. The enhanced activity of PMHs **4**, **9**, and **29** may also be attributed to the presence of bulky groups in *p*-position, which is surrounded by green contours in steric field plot. The sterically unfavored yellow regions were observed near the *o*-position of benzylidine group at the opposite direction of *N*-1 of hydantoin moiety.

CoMFA electrostatic fields are shown as blue (more positive charge) and red (more negative charge) polyhedra in Figure 5B.

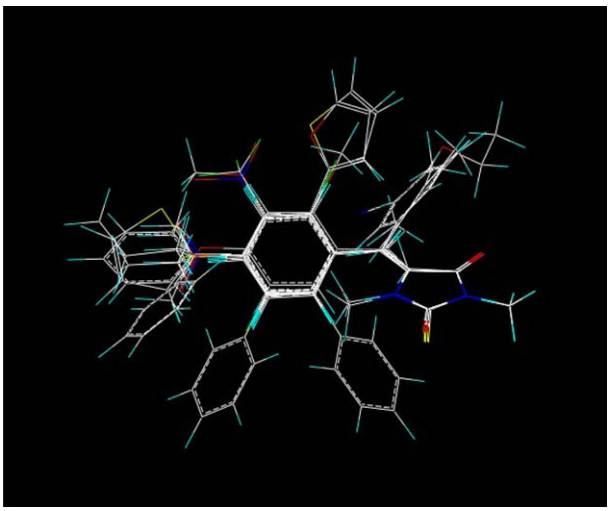

Figure 4. Superposition of PMHs training and test sets using field fit alignment.

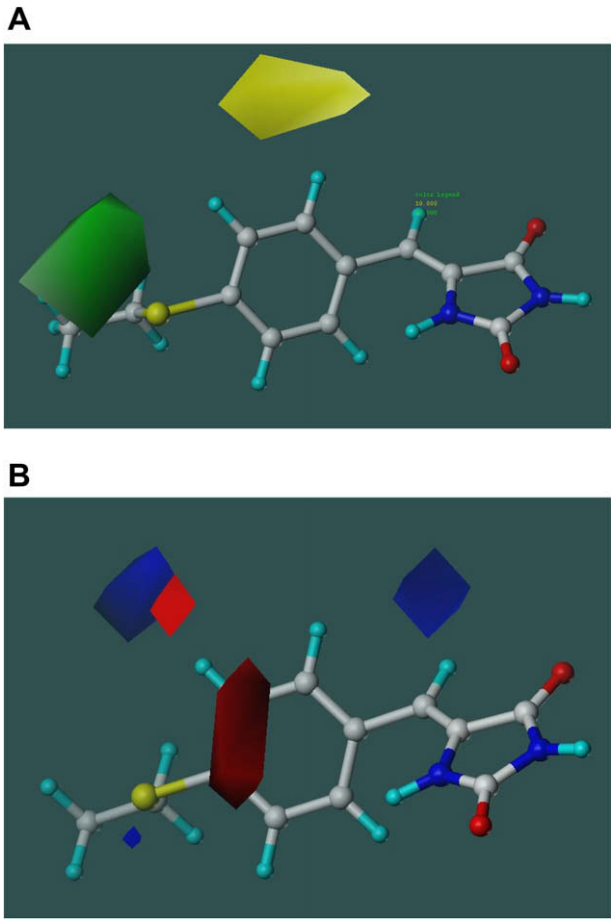

Figure 5. Graphical representation of CoMFA STDEV* COEFF analysis based field fit alignment. (A) Steric contour plots: Sterically favored (80% contribution level) are represented by green polyhedra predicted to increase activity. Sterically disfavored (10% contribution level) are represented by yellow polyhedra predicted to decrease activity. (B) Electrostatic contour plots: Negative charge-favored areas (80% contribution level) are represented by red polyhedra. Negative charge-disfavored areas (20% contribution level) are represented by blue polyhedra.

Though the electrostatic field contributions are less, a small change in electrostatic interaction will have a considerable effect on the activity. Red contour was observed near *m*- and *p*-positions of the phenyl ring of **4**. Therefore, compounds possessing electronegative groups near these regions (high electron density) may show more activity. The distal part of the benzylidene group have an electronegative group with prominent red contour, which is consistent with the observation that the three most active PMHs with migration values less than 30 μm (**22**, **29** and **4**) posses oxygen, nitrogen and sulfur atoms, respectively in the *p*-position. These compounds have H-accepting properties that could contribute to hydrogen bonding interaction near this position. Blue contours reside around the upper right-hand and upper left-hand corners of **4**, which brace the hydrogen atoms of the aromatic and ethylene moieties, indicating that electropositive groups near this area are predicted to increase the activity. This could also be a possible indication that H-bond donor groups in this position could be favored. The red contours near the *p*-position of the benzylidene group coincide with the sterically favorable green contours. Therefore, substituents at these positions should be electron-donating but with high steric bulk for better activity. Blue contour at the *o*-position of benzylidene group was observed. Therefore, a low electron density in this area will have a positive effect on the anti-metastatic activity. Due to the low substitution variability in the training set around the hydantoin ring, no contours were observed in this area.

In conclusion, PMH is a novel anti-metastatic lead class that can be easily, regioselectively, and cost effectively synthesized. These advantages bode well for the emergence of future PMHs as potential therapeutics for the control and prevention of metatstatic prostate cancer.

3. Experimental

3.1. General experimental procedures

IR spectra were recorded on a Varian 800 FT-IR spectrophotometer. Optical rotation measurements were carried out on a Rudolph Research Analytical Autopol III polarimeter. TLC analyses were carried out on precoated silica gel 60 F_{254} 500 μm TLC plates, using MeOH/$CHCl_3$ (1:9) as a developing solvent. For CC, Si gel 60 (particle size 63–200 μm) was used. The ^1H and ^{13}C NMR spectra were recorded in DMSO-d_6, using TMS as an internal standard, on a JEOL Eclipse NMR spectrometer operating at 400 MHz for ^1H and 100 MHz for ^{13}C. The HREIMS experiments were conducted at the University of Michigan on a Micromass LCT spectrometer. Molecular modeling and CoMFA studies were performed using the SYBYL 8.0 suit of programs (Tripos Discovery Informatics, St. Louis, Missouri) installed on a DELL desktop workstation equipped with a 1.8 GHz Intel® Xeon® processor running the Red Hat Enterprise Linux (version 4) operating system. The chemical structures of hydantoin derivatives were sketched in SYBYL 8.0 and assigned Gasteiger partial charges and energy minimized using Energy Force Field to a final root-mean-square gradient of 0.01 kcal/mol.

3.2. Animal material

The sponge *Hemimycale arabica* was collected at a depth of −10 m in June 2003 using SCUBA from Desha, 12.4 miles south of Hurghada at the Egyptian Red Sea coast. The sponge is dark blue from the exterior with greenish yellow linings at its interior. Encrusted form of this sponge has crumbly texture with smooth surface, and it usually builds thin layer of crust and covers an area approximately equal to 15 cm. Its thickness varies between several mm to 2.5 cm and hence its growth forms are sometimes more cushion-like. Areolated pore fields were present on the surface of sponge which forms minor depressions, and oscules are also present which are raised in to the small tubes having 1–5 mm in diameter and are irregularly distributed over the entire surface. A

voucher was deposited in the collections of the Zoological Museum of the University of Amsterdam under the registration number ZMAPOR19764.

3.3. Extraction and isolation

About 1 kg frozen sponge was blended with EtOH and filtered. The blended sponge material was extracted with EtOH at room temperature (4 × 2 L). Ethanolic extracts were pooled and then evaporated under vacuum. The dried extract (~32.0 g) was then subjected to Si gel 60 (1 kg, <63 μm) medium pressure liquid chromatography (MPLC) using $CHCl_3$–MeOH gradient elution to afford several fractions containing phenylmethylene hydantoins. Pooled fractions were further chromatographed on Si gel 60 using $CHCl_3$–MeOH gradient elution. Final purification was achieved on C-18 Si gel (Bakerbond, Octadecyl, 40 μm) with H_2O–MeOH gradient elution or Sephadex LH-20 using $CHCl_3$–MeOH gradient elution.

3.4. Preparation of semisynthetic phenylmethylene hydantoins

Hydantoin (1.0 gm) was dissolved in 10 mL H_2O while heating at 70 °C on oil bath with continuous stirring (Scheme 1).[11] After complete dissolution, the pH was adjusted to 7.0 using saturated $NaHCO_3$ solution. The temperature was then raised to 90 °C after the addition of 0.9 mL ethanolamine.[11] An equimolar quantity of the corresponding aldehyde solution in 2–5 mL EtOH was added drop wise with continuous stirring.[11] The reaction was kept under reflux for approximately 5–8 h. The reaction was monitored by TLC every hour after a yellow or white precipitate is formed. After complete depletion of the starting material, the mixture was cooled and the precipitate was filtered and washed with EtOH/H_2O (1:5) before recrystallization from EtOH.[11] Reaction yield range from 60-90%, based on the nature of the used aldehyde.

3.5. Spheroid disaggregation assay

Spheroids were prepared from single cell suspension of PC-3M prostate cancer cell line as described before.[29,30,33,34] In brief, 5×10^4/mL cells in RPMI 1640 serum-free medium were placed on 96-well low-attachment tissue culture plates. The plates were rocked on a gyrorotatory shaker in a CO_2 incubator at 37 °C for 2 days, at the end of which the spheroids measuring 150–300 μm in diameter (~4×10^4 cells/spheroid) were formed. A single spheroid was then placed in the center of each well of ECM-coated 24-well microplate in 200 μL of serum-free medium.[29,30,33,34] Previous studies determined that 1 h is an appropriate time for spheroids to begin adhering to an ECM. Thus $t = 0$ was set as 1 h from initial plating, so that if the plate was not disturbed, the spheroids would not move from their location at the time of plating. Spheroids were photographed digitally at $t = 0$, cultured at 37 °C for 48 h, and then re-photographed. The spheroids were then fixed, stained with Diff-Quik™ (Dade Behring, Newark, DE) and examined under light microscopy. The diameter of the area covered with cells migrated from the spheroids was measured in a microscope calibrated with a stage and ocular micrometer. The radial distance of migration was calculated after subtraction of the mean initial spheroidal diameter at $t = 0$. PMHs **1** and **4** were tested at multiple doses ranging from 0 to 500 μM and each dose was tested in triplicate. Values shown represent the average percent increase in surface area of spheroids.[29,30,33,34]

3.6. Design of 3D QSAR model

A data set of 35 PMH derivatives was used for this study. The anti-metastatic activity for these compounds was determined using PC-3M spheroid disaggregation assay. The activity was expressed as migration distance in μm (Tables 5 and 6). The ($-\log EC_{50}$) which is the concentration required to decrease migration distance by 50% was used in CoMFA.

To evaluate the predictability of the generated 3D QSAR model, PMHs were divided into training set and test set. Each set possessed PMH analogs with a similar range of anti-metastatic activity. Thus, the test set is the true representative of the training set. This was achieved by arbitrarily setting aside 6 compounds as a test set with a regularly distributed anti-metastatic activity. The mean (standard deviation) of the activity of the training and test set was 96.32 (40.04) and 87.67 (57.18), respectively. Tables 5 and 6 show the actual and predicted activity for both training and test sets, respectively.[35,36] The predicted activities of training and test set values were obtained by multiplying the values of each descriptor for a particular row generated by CoMFA by its corresponding coefficient from the PLS equation in the model.[35]

3.6.1. Alignment rule

The alignment rule, that is, molecular conformation and orientation, is one of the most sensitive input areas for CoMFA studies.[35,36] The SYBYL QSAR rigid body field fit command was used for this alignment. Field fit uses a Simplex algorithm in SYBYL that minimizes the differences in steric and electrostatic fields averaged over all the lattice grid points to find the best fit. One of the most active PMHs **4** was used as a reference compound, on which other molecules were aligned. This fit is dependent on the similarity and initial orientations of the molecules. Values of the steric and electrostatic fields were truncated at 30 kcal/mol. The aligned PMHs are shown in Figure 4.

3.6.2. Partial least square (PLS) analysis

The partial least squares algorithm was used in conjugation with the cross-validation (leave-one-out) option to obtain the optimum number of components which were used to generate the final CoMFA model without cross-validation.[35,36] The result from a cross-validated analysis was expressed as q^2, which is defined as $q^2 = 1 - \text{PRESS}/\sum(Y - Y_{\text{mean}})^2$ where $\text{PRESS} = \sum(Y - Y_{\text{Pred}})^2$. The q^2 can take up values in the range from 1, suggesting a perfect model, to less than 0, where the errors of prediction are greater than the error from assigning each compound mean activity of the model. Cross validated PLS analysis using the leave-one-out procedure employed 6 components, in which each compound is systematically excluded from the set and its activity was predicted by a model derived from the rest of the compounds. Thus cross validation by the leave-one-out method evaluates the model not by how it best fits the data but by how it best predicts the data.[35,36] The optimum number of components was defined as that which yielded the highest q^2 value, which normally had the smallest RMS error of prediction (SEP). Equal weights were assigned to the steric and electrostatic descriptors using the CoMFA_STD scaling option. The final PLS analysis was then performed using the optimum number of components with no cross-validation. The final PLS analysis was then performed using the optimum number of components with no cross-validation. To obtain the statistical confidence limits on the analysis, PLS analysis using 100 bootstrap (bs) groups with the optimum number of components was performed.[35,36]

3.6.3. Predictive r^2 values

The predictive ability was determined from a set of 6 compounds that were not included in the training set (Table 6). These compounds were aligned, and their activities were predicted by PLS analysis. The predictive r^2 (r^2pred) value was based on PMHs of the test set only and is defined as where SD is the sum of the squared deviations between the anti-metastatic activities of the test set and mean activity of the training set molecules and PRESS

is sum of the squared deviation between predicted and actual activity values for every molecule in the test set.[35,36]

3.7. (*Z*)-5-(4-(Ethylthio)benzylidene)imidazolidine-2,4-dione (4)

Yellow amorphous solid, IR ν_{max} ($CHCl_3$) 3382, 1721, 1645, 1592 cm^{-1}; ^1H and ^{13}C NMR see Tables 1 and 2; HREIMS *m*/*z* 248.0622 $[M]^+$ (calcd for $C_{12}H_{12}N_2O_2S$, 248.0619).

3.8. (*Z*)-5-(2,3-Difluoro-4-methylbenzylidene)imidazolidine-2,4-dione (5)

White amorphous solid, IR ν_{max} ($CHCl_3$) 3235, 1742, 1674 cm^{-1}; ^1H and ^{13}C NMR see Tables 1 and 2; HREIMS *m*/*z* 238.0559 $[M]^+$ (calcd for $C_{11}H_8F_2N_2O_2$, 238.0554).

3.9. (*Z*)-5-(Biphenyl-2-ylmethylene)imidazolidine-2,4-dione (6)

Yellow amorphous solid, IR ν_{max} ($CHCl_3$) 1769, 1714, 1650 cm^{-1}; ^1H and ^{13}C NMR see Tables 1 and 2; HREIMS *m*/*z* 264.0894 $[M]^+$ (calcd for $C_{16}H_{12}N_2O_2$, 264.0899).

3.10. (*Z*)-5-(Biphenyl-3-ylmethylene)imidazolidine-2,4-dione (7)

Yellow amorphous solid, IR ν_{max} ($CHCl_3$) 3439, 3258, 1771, 1727, 1663 cm^{-1}; ^1H and ^{13}C NMR see Tables 1 and 2; HREIMS *m*/*z* 264.0898 $[M]^+$ (calcd for $C_{16}H_{12}N_2O_2$, 264.0899).

3.11. (*Z*)-5-(2-(Thiophen-2-yl)benzylidene)imidazolidine-2,4-dione (8)

Yellow amorphous solid, IR ν_{max} ($CHCl_3$) 3441, 3227, 1771, 1728, 1663 cm^{-1}; ^1H and ^{13}C NMR see Tables 3 and 4; HREIMS *m*/*z* 270.0452 $[M]^+$ (calcd for $C_{14}H_{10}N_2O_2S$, 270.0463).

3.12. (*Z*)-5-(4-(Thiophen-2-yl)benzylidene)imidazolidine-2,4-dione (9)

Yellow amorphous solid, IR ν_{max} ($CHCl_3$) 3288, 3229, 1779, 1730, 1660 cm^{-1}; ^1H and ^{13}C NMR see Tables 3 and 4; HREIMS *m*/*z* 270.0455 $[M]^+$ (calcd for $C_{14}H_{10}N_2O_2S$, 270.0463).

3.13. (*Z*)-5-(2-(Furan-2-yl)benzylidene)imidazolidine-2,4-dione (10)

Brown amorphous solid, IR ν_{max} ($CHCl_3$) 3433, 3184, 1771, 1729, 1662; ^1H and ^{13}C NMR see Tables 3 and 4; HREIMS *m*/*z* 254.0689 $[M]^+$ (calcd for $C_{14}H_{10}N_2O_3$, 254.0691).

3.14. (*Z*)-5-(3-(Cyano)benzylidene)imidazolidine-2,4-dione (11)

Yellow amorphous solid, IR ν_{max} ($CHCl_3$) 3383, 3317, 2235, 1729, 1662, 1602 cm^{-1}; ^1H and ^{13}C NMR see Tables 3 and 4; HREIMS *m*/*z* 213.0530 $[M]^+$ (calcd for $C_{11}H_7N_3O_2$, 213.0538).

Acknowledgments

This investigation was made possible through the support of NIH Grants P20RR16456 from the BRIN Program of the National Center for Research Resources, and R01CA96534 (G.V.S.).

References and notes

1. Jemal, A.; Rebecca Siegel, R.; Ward, E.; Hao, Y.; Xu, J.; Murray, T.; Thun, M. J. *CA Cancer J. Clin.* **2008**, *58*, 71–96.
2. Fleshner, N.; Zlotta, A. R. *Cancer* **2007**, *110*, 1889–1899.
3. Louwrier, S.; Ostendorf, M.; Boom, A.; Hiemstra, H.; Speckamp, W. N. *Tetrahedron* **1996**, *52*, 2603–2628.
4. Ohtani, I.; Kusumi, T.; Kakisawa, H.; Kashman, Y.; Hirsh, S. *J. Am. Chem. Soc.* **1992**, *114*, 8472–8479.
5. Kashman, Y.; Hirsh, S.; McConnell, O. J.; Ohtani, I.; Kusumi, T.; Kakisawa, H. *J. Am. Chem. Soc.* **1989**, *111*, 8925–8926.
6. Boyd, W. J.; Robson, W. *Biochem. J.* **1935**, *29*, 542–545.
7. Sutherland, J. J.; Weaver, D. F. *J. Chem. Inf. Comput. Sci.* **2003**, *43*, 1028–1036.
8. Djura, P.; Stierle, D. B.; Sullivan, B.; Faulkner, D. J.; Arnold, E. V.; Clardy, J. *J. Org. Chem.* **1980**, *45*, 1435–1441.
9. Perry, T. L. Isolation and Lead Optimization of Natural Sunscreens from the Marine Sponge *Laxosubrites* sp. A Master's Thesis, The University of Mississippi, University, Mississippi, 1998, 28–40.
10. Shah, G. V.; Muralidharan A.; Thomas, S.; Gokulgandhi, M.; Mudit, M.; Khanfar, M.; El Sayed, K. A. *Mol. Cancer Ther.* **2009**, *8*, in press.
11. Thenmozhiyal, J. C.; Wong, P. T.; Chui, W. K. *J. Med. Chem.* **2004**, *47*, 1527–1535.
12. Meuesel, M.; Gutschow, M. *Org. Prep. Proced. Int.* **2004**, *36*, 391–443.
13. Naohiro, I.; Tadayoshi, S.; Ikuo, K.; Katsuji, Y.; Yutaka, A.; Toshiaki, Y. *Jpn. Kokai Tokkyo Koho*, **1987**, JP 62029570. *Chem. Abstr.* **1987**, *106*, 213918.
14. Shapiro, P.; Mackerell, A. D. U.S. Pat. Appl. Publ. 666206; *Chem. Abstr.* **2006**, *146*, 330819.
15. Koenig W.; Zoller G.; Just M.; Jablonka B. Preparation of Peptide Hydantoin Derivatives as Drugs. Ger. Offen. 1993, Application: DE 91-4126277 19910808. CAN 119:181238.
16. Carmi, C.; Cavazzoni, A.; Zuliani, V.; Lodola, A.; Bordi, F.; Plazzi, P. V.; Alfieri, R. R.; Petronini, P. G.; Mor, M. *Bioorg. Med. Chem. Lett.* **2006**, *16*, 4021–4025.
17. Newman, D. J.; Cragg, G. M. *J. Nat. Prod.* **2007**, *70*, 461–477.
18. Newman, D. J.; Cragg, G. M. In *Bioactive Natural Products*; Colegate, S. M., Molyneux, R. J., Eds., 2nd ed.; CRC Press: Boca Raton, Florida, 2008; pp 323–370.
19. McChesney, J. D.; Venkataraman, S. K.; Henri, J. T. *Phytochemistry* **2007**, *68*, 2015–2022.
20. Cortes, S.; Liao, Z. K.; Watson, D.; Kohn, H. *J. Med. Chem.* **1985**, *28*, 601–606.
21. Brown, M. L.; Brown, G. B.; Brouillette, W. J. *J. Med. Chem.* **1997**, *40*, 602–607.
22. Wong, P. T. H.; Tan, S. F. *Jpn. J. Pharmacol.* **1989**, *49*, 309–315.
23. Rozen, S.; Ben-Shushan, G. *Magn. Reson. Chem.* **1985**, *23*, 116–118.
24. Singh, R. D.; Singh, S. N. *J. Magn. Reson.* **1974**, *16*, 110–114.
25. Silverstein, R. M.; Webster, F. X.; Kiemle, D. J. In *Spectrometric Identification of Organic Compounds*, 7th ed.; John Wiley & Sons: Hoboken, NJ, 2005; p 103.
26. Hirohashi, S.; Kanai, Y. *Cancer Sci.* **2003**, *94*, 575–581.
27. Cohen, M. B.; Griebling, T. L.; Ahaghotu, C. A.; Rokhlin, O. W.; Ross, J. S. *Am. J. Clin. Pathol.* **1997**, *107*, 56–63.
28. Balda, M. S.; Matter, K. *Semin. Cell Dev. Biol.* **2000**, *11*, 281–289.
29. Thomas, S.; Chigurupati, S.; Anabalagan, M.; Shah, G. V. *Mol. Endocrinol.* **2006**, *20*, 1894–1911.
30. Sabbisetti, V. S.; Chirugupati, S.; Thomas, S.; Vaidya, K. S.; Reardon, D.; Chiriva-Internati, M.; Iczkowski, K. A.; Shah, G. V. *Int. J. Cancer* **2005**, *117*, 551–560.
31. Chien, J.; Wong, E.; Nikes, E.; Noble, M. J.; Pantazis, C. G.; Shah, G. V. *Oncogene* **1999**, *18*, 3376–3382.
32. Thomas, S.; Chiriva-Internati, M.; Shah, G. V. *Clin. Exp. Metastasis* **2007**, *24*, 363–377.
33. Heuser, M.; Ringert, R. H.; Zoeller, G.; Hemmerlein, B. *J. Urol.* **2003**, *169*, 1267–1270.
34. Hoevel, T.; Macek, R.; Swisshelm, K.; Kubbies, M. *Int. J. Cancer* **2004**, *108*, 374–383.
35. Cramer, R. D., III; Patterson, D. E.; Bunce, J. D. *J. Am. Chem. Soc.* **1988**, *110*, 5959–5967.
36. Bohm, M.; Sturzebecher, J.; Klebe, G. *J. Med. Chem.* **1999**, *42*, 458–477.